

Advances in Computer Vision

Michal Haindl  
Jiří Filip

Visual

Accurate Material A

# **Advances in Computer Vision and Pattern Recognition**

For further volumes:  
[www.springer.com/series/4205](http://www.springer.com/series/4205)

Michal Haindl • Jiří Filip

# Visual Texture

Accurate Material Appearance  
Measurement, Representation  
and Modeling

 Springer

Michal Haindl  
Inst. of Information Theory & Automation  
Acad. of Sciences of the Czech Republic  
Prague, Czech Republic

Jiří Filip  
Inst. of Information Theory & Automation  
Acad. of Sciences of the Czech Republic  
Prague, Czech Republic

*Series Editors*

Prof. Sameer Singh  
Research School of Informatics  
Loughborough University  
Loughborough  
UK

Dr. Sing Bing Kang  
Microsoft Research  
Microsoft Corporation  
Redmond, WA  
USA

ISSN 2191-6586

Advances in Computer Vision and Pattern Recognition

ISBN 978-1-4471-4901-9

DOI 10.1007/978-1-4471-4902-6

Springer London Heidelberg New York Dordrecht

ISSN 2191-6594 (electronic)

ISBN 978-1-4471-4902-6 (eBook)

Library of Congress Control Number: 2013930058

© Springer-Verlag London 2013

This work is subject to copyright. All rights are reserved by the Publisher, whether the whole or part of the material is concerned, specifically the rights of translation, reprinting, reuse of illustrations, recitation, broadcasting, reproduction on microfilms or in any other physical way, and transmission or information storage and retrieval, electronic adaptation, computer software, or by similar or dissimilar methodology now known or hereafter developed. Exempted from this legal reservation are brief excerpts in connection with reviews or scholarly analysis or material supplied specifically for the purpose of being entered and executed on a computer system, for exclusive use by the purchaser of the work. Duplication of this publication or parts thereof is permitted only under the provisions of the Copyright Law of the Publisher's location, in its current version, and permission for use must always be obtained from Springer. Permissions for use may be obtained through RightsLink at the Copyright Clearance Center. Violations are liable to prosecution under the respective Copyright Law.

The use of general descriptive names, registered names, trademarks, service marks, etc. in this publication does not imply, even in the absence of a specific statement, that such names are exempt from the relevant protective laws and regulations and therefore free for general use.

While the advice and information in this book are believed to be true and accurate at the date of publication, neither the authors nor the editors nor the publisher can accept any legal responsibility for any errors or omissions that may be made. The publisher makes no warranty, express or implied, with respect to the material contained herein.

Printed on acid-free paper

Springer is part of Springer Science+Business Media ([www.springer.com](http://www.springer.com))

*To our families, for their continuous support*

# Preface

The main purpose of this book is to provide a comprehensive state-of-the-art survey of the newly emerging area of physically correct visual texture modeling. Multi-dimensional visual texture is the appropriate paradigm for physically correct representation of material visual properties. The book presents recent advance in the texture modeling methodology used in computer vision, pattern recognition, computer graphics, and virtual and augmented reality applications.

While texture analysis is a well-established research field, it is still predominantly restricted to the simplest and most approximate texture representation—either gray-scale or color textures. Several books devoted to such simple static texture analysis have been published, but there is no book dedicated to either the area of more general texture modeling or recent state-of-the-art textural representations.

Several features set our book apart from the few other visual texture books published.

- The only book with comprehensive treatment of texture synthesis.
- The only book covering all known aspects of the most advanced visual surface representation which can be recently applied—the Bidirectional Texture Function (BTF).
- The right timing. This book arrives at a time of advanced computing and graphics hardware which can process and store enormous amounts of data needed for physically correct material modeling and recognition; likewise, recent GPU programming progress allows users to utilize relatively intuitive and economical programming. This allows for fast implementation, thereby enabling real industrial applications of the presented methods.
- A complete reference. This self-contained book covers the entire pipeline from material appearance representation, measurement, analysis, and compression, to modeling, editing, visualization, and perceptual evaluation.

Recent progress in computing and acquisition technology of advanced visual data, together with advances in theories of mathematical modeling, provide us with timely opportunity to achieve new breakthroughs beyond the current state of computer vision art. Finally, it is possible to measure not only the ordinary static color

textures, but also the far more complicated and accurate high-dimensional visual texture representations.

Natural visual textures provide ample information about local lighting field structure as well as the surface relief, accounting for such effects as self-occlusions, self-shadowing, inter-reflection or subsurface scattering. Moreover, the appearance of real materials dramatically changes with, for example, illumination and viewing variations. The prevailing computer vision methodology uses only a small fraction of this readily available and potentially rich information source, but we believe that this emerging research area will soon have significant impacts on further progress in artificial visual cognition and related applications. Our aim is thus to offer the first book with this focus, in order to foster this development.

The book builds on the authors' work in this field over two decades and was inspired by positive feedback to several of our tutorials: *Bidirectional Texture Function Modelling* at CVPR 2010, San Francisco, *Accurate Material Appearance Modelling* at SCIA 2011, Ystad, *Advanced Textural Representation of Materials Appearance* at SIGGRAPH 2011, Hong Kong, and *Advanced Nature Exteriors Modelling* at ICPR 2012, Tsukuba.

The book starts from the basic principles and builds on the fundamentals and basic visual texture taxonomy introduced as a foundation for using the latest techniques in texture modeling. The reader is expected to possess graduate level knowledge in statistics and probability theory as well as competence in basic computer graphics principles. However, it is also suitable for newcomers to the field of computer graphics and computer vision, as well as for practitioners who wish to be brought up to date on the state-of-the-art methodology of texture modeling. This survey book will provide a useful reference and textbook for researchers, lecturers, industry practitioners, and students interested in this new and progressive research area.

We tried to keep the book as concise as possible to maintain its scope at an acceptable level. Rather than explaining mathematical and implementation details of all methods, we refer to the original publications. Our ambition was to provide the reader with general knowledge about state-of-the-art visual texture modeling. Attempting to rigorously explain, for example, the Markovian or mixture models used in this book would require at least twice as many pages.

Prague, Czech Republic

Michal Haindl  
Jiří Filip

# Acknowledgements

Many colleagues from the department of Pattern Recognition of the Institute of Information Theory and Automation of the Academy of Sciences of the Czech Republic in Prague have contributed invaluable parts to this work in our joint publications or doing some experimental work. We would like to thank Dr. Jiří Grim, Martin Hatka, Michal Havlíček, Dr. Vojtěch Havlíček, Radek Holub, Dr. Stanislav Mikeš, Václav Remeš, Dr. Petr Somol, Dr. Pavel Vácha, Radomír Vávra, and Dr. Pavel Žid.

We are also grateful for many stimulating discussions to colleagues—Prof. Michael J. Chantler, Prof. Patrick R. Green from the Heriot-Watt University, Prof. Reinhard Klein from the Bonn University, Dr. Giuseppe Scarpa from the University Federico II, and Prof. Mineichi Kudo from the Hokkaido University.

We would like also to thank Bonn University and Yale University for providing us some BTF measurements used in this book, DaimlerChrysler AG for 3D model of car interior, various participants for taking part in the psycho-physical experiments, and for the partial support of the Czech Science Foundation projects 102/08/0593, 103/11/0335.

Finally, we would like to thank our families for their support and patience during many years of research leading to this book.

# Contents

<b>1</b>	<b>Motivation</b>	1
1.1	Visual Texture Definition	1
1.2	Contents Overview	6
	References	7
<b>2</b>	<b>Representation</b>	9
2.1	General Reflectance Function	9
2.2	Textured Model Representation Taxonomy	12
2.2.1	Bidirectional Surface Scattering Reflectance Distribution Function	12
2.2.2	Bidirectional Reflectance and Transmittance Texture Function	13
2.2.3	Bidirectional Texture Function	14
2.2.4	Spatially Varying BRDF	14
2.2.5	Surface Light Field	15
2.2.6	Surface Reflectance Field	16
2.2.7	Multispectral Texture	16
2.3	Representation Taxonomy of Homogeneous Models	17
2.3.1	Bidirectional Scattering Distribution Function	18
2.3.2	Bidirectional Reflectance Distribution Function	18
2.3.3	Bidirectional Transmittance Distribution Function	19
2.3.4	Isotropic Bidirectional Reflectance Distribution Function	20
2.4	Attributes of Taxonomical Classes	21
2.4.1	Taxonomical Class Advantages	21
2.4.2	Taxonomical Class Drawbacks	22
	References	22
<b>3</b>	<b>Texture Acquisition</b>	23
3.1	High Dynamic Range Texture Acquisition	23
3.2	Static Textures Acquisition	24

3.3	Dynamic Textures Acquisition . . . . .	25
3.4	BRDF Acquisition . . . . .	26
3.4.1	Gonioreflectometers-Based BRDF Setups . . . . .	28
3.4.2	Mirror-Based BRDF Setups . . . . .	30
3.4.3	Image-Based BRDF Acquisition . . . . .	32
3.4.4	Portable BRDF Acquisition Systems . . . . .	34
3.5	Spatially Varying BRDF Acquisition . . . . .	35
3.6	BTF Acquisition . . . . .	37
3.6.1	Gonioreflectometers-Based BTF Setups . . . . .	38
3.6.2	Mirror-Based BTF Setups . . . . .	42
3.6.3	Other BTF Setups . . . . .	42
3.6.4	Sparse Sampling of BTF . . . . .	43
3.6.5	BTF Setups Overview . . . . .	44
3.6.6	A BTF Setup Design . . . . .	44
3.7	Measurement of Time-Varying Surfaces . . . . .	47
3.8	BSSRDF Measurement . . . . .	48
3.8.1	Diffuse-Specular Separation of Reflectance Measurements . . . . .	48
3.8.2	Homogeneous Subsurface Scattering Measurement . . . . .	50
3.8.3	Spatially Varying Subsurface Scattering Measurement . . . . .	51
3.9	Surface Light and Reflectance Fields Measurements . . . . .	53
	References . . . . .	55
<b>4</b>	<b>Static Multispectral Textures . . . . .</b>	<b>63</b>
4.1	Texture Modeling Approaches . . . . .	63
4.2	Model-Based Representations . . . . .	64
4.2.1	Spectral Factorization . . . . .	65
4.2.2	Spatial Factorization . . . . .	66
4.2.3	Fractal Models . . . . .	67
4.2.4	Random Mosaics . . . . .	68
4.2.5	Markovian Models . . . . .	70
4.2.6	Mixture Models . . . . .	80
4.2.7	Probabilistic Discrete-Mixture 2D Model . . . . .	83
4.2.8	Bernoulli Distribution Mixture Model . . . . .	84
4.2.9	Gaussian-Mixture 2D Model . . . . .	85
4.2.10	Mixture Model-Based Texture Synthesis . . . . .	86
4.2.11	Probabilistic Mixture Models Properties . . . . .	87
4.3	Texture Sampling . . . . .	88
4.3.1	Texture Sampling Methods . . . . .	88
4.3.2	Roller . . . . .	89
4.3.3	Sampling Methods Summary . . . . .	89
4.4	Hybrid Modeling . . . . .	90
	References . . . . .	92
<b>5</b>	<b>Dynamic Textures . . . . .</b>	<b>97</b>
5.1	Introduction . . . . .	97

- 5.2 Modeling Approaches . . . . . 98
  - 5.2.1 Sampling Methods . . . . . 98
  - 5.2.2 Mathematical Models . . . . . 100
- 5.3 Adaptive Models . . . . . 101
  - 5.3.1 Learning . . . . . 101
  - 5.3.2 Synthesis . . . . . 102
  - 5.3.3 Spatio-Temporal Autoregressive Model . . . . . 102
  - 5.3.4 Multiscale Autoregressive Model . . . . . 102
  - 5.3.5 Autoregressive Eigen Model . . . . . 103
  - 5.3.6 Linear Dynamical System . . . . . 105
  - 5.3.7 Time-Varying LDS . . . . . 107
  - 5.3.8 Switching Linear Dynamical System . . . . . 108
  - 5.3.9 Mixture of LDSs . . . . . 109
  - 5.3.10 Region-Based LDS . . . . . 109
  - 5.3.11 Non-parametric Dynamic Model . . . . . 109
  - 5.3.12 Nonlinear Dynamical System . . . . . 110
- 5.4 DT Test Data . . . . . 111
- 5.5 Quality Validation . . . . . 112
- 5.6 Other Applications . . . . . 113
- 5.7 Summary . . . . . 113
- References . . . . . 114
  
- 6 Spatially Varying Bidirectional Reflectance Distribution**
- Functions** . . . . . 119
  - 6.1 BRDF Principle and Properties . . . . . 119
  - 6.2 BRDF Representations . . . . . 121
  - 6.3 BRDF Compression . . . . . 124
  - 6.4 BRDF Models . . . . . 126
    - 6.4.1 Ideal Mirror and Diffuse Reflection . . . . . 127
    - 6.4.2 Empirically Derived Reflectance Models . . . . . 128
    - 6.4.3 Physically Motivated BRDF Models . . . . . 132
    - 6.4.4 Probabilistic BRDF Models . . . . . 136
    - 6.4.5 Multilayer BRDF Models . . . . . 136
    - 6.4.6 BRDF Models Comparison . . . . . 137
  - 6.5 BRDF Extension to Spatially Varying BRDF . . . . . 138
    - 6.5.1 Approximative SVBRDF Measurement . . . . . 139
  - 6.6 BRDF and SVBRDF Editing Methods . . . . . 141
- References . . . . . 142
  
- 7 Bidirectional Texture Functions** . . . . . 147
  - 7.1 BTF Representations . . . . . 147
  - 7.2 BTF Methods Taxonomy . . . . . 148
  - 7.3 BTF Dimensionality Analysis . . . . . 148
    - 7.3.1 Statistical Methods . . . . . 149
    - 7.3.2 Psychophysical Methods . . . . . 152
  - 7.4 Compression Methods . . . . . 152

7.4.1	Pixel-Wise Compression . . . . .	154
7.4.2	Linear Factorization Approaches . . . . .	156
7.4.3	Clustering Approaches . . . . .	159
7.4.4	Approaches Combining Surface Geometry and Reflectance . . . . .	160
7.4.5	Other Approaches . . . . .	160
7.5	Modeling Methods . . . . .	161
7.5.1	Sampling Methods . . . . .	162
7.5.2	Spatial Enlargement of BTF Reflectance Models . . . . .	166
7.5.3	Statistical Models . . . . .	174
7.5.4	Hybrid Methods . . . . .	183
7.5.5	Compound Methods . . . . .	185
7.6	BTF Editing . . . . .	186
7.7	Comparison of Selected Methods . . . . .	187
7.7.1	Tested Methods Description . . . . .	187
7.7.2	A Psychophysical Comparison . . . . .	192
7.7.3	Computational and Visual Quality Comparison . . . . .	195
7.7.4	Parametric Representation Size and Compression . . . . .	197
7.7.5	Speed Comparison . . . . .	201
7.7.6	Discussion . . . . .	202
7.8	Summary . . . . .	203
	References . . . . .	205
<b>8</b>	<b>Visualization . . . . .</b>	<b>211</b>
8.1	Introduction . . . . .	211
8.2	Texture Mapping . . . . .	212
8.3	World vs. Local Coordinate Systems . . . . .	213
8.4	Local Coordinate System . . . . .	214
8.4.1	Barycentric Coordinates . . . . .	216
8.5	Surface Height Simulation . . . . .	217
8.5.1	Bump Mapping . . . . .	217
8.5.2	Displacement Mapping . . . . .	220
8.6	Measured Direction Interpolations . . . . .	220
8.7	Directional Appearance Rendering . . . . .	222
8.8	Illumination Environment . . . . .	223
8.9	Texture Anti-aliasing . . . . .	225
8.10	Rendering Using Graphics Hardware . . . . .	226
	References . . . . .	228
<b>9</b>	<b>Perceptual Validation and Analysis . . . . .</b>	<b>231</b>
9.1	Motivation . . . . .	231
9.2	Texture Similarity Computational Measures . . . . .	232
9.2.1	Local Similarity Measures . . . . .	232
9.2.2	Statistical Similarity Measures . . . . .	236
9.3	Visual Psychophysics . . . . .	238
9.3.1	Stimuli Preparation . . . . .	239

- 9.3.2 Data Analysis . . . . . 240
- 9.3.3 Perceptual Texture Space . . . . . 241
- 9.3.4 BRDF Visual Perception . . . . . 243
- 9.3.5 Perceptually Driven BTF Analysis and Compression . . . . . 245
- References . . . . . 250
- 10 Applications . . . . . 255**
  - 10.1 Applied Visual Textures . . . . . 255
  - 10.2 Editing . . . . . 256
  - 10.3 Visual Scene Interpretation . . . . . 259
    - 10.3.1 Segmentation . . . . . 259
    - 10.3.2 Visual Invariants . . . . . 261
    - 10.3.3 Medical Applications . . . . . 264
    - 10.3.4 Security . . . . . 265
  - 10.4 Human Perception . . . . . 267
  - 10.5 Correct Visualization of Visual Scenes . . . . . 267
    - 10.5.1 Movie and Game Industry . . . . . 268
    - 10.5.2 Car Industry . . . . . 268
    - 10.5.3 Cultural Heritage Preservation . . . . . 269
  - References . . . . . 273
- 11 Conclusions and Open Problems . . . . . 277**
  - 11.1 Visual Texture . . . . . 277
  - 11.2 Measurement . . . . . 278
  - 11.3 Mathematical Models . . . . . 278
  - 11.4 Validation . . . . . 279
  - 11.5 Real-Time Visualization . . . . . 279
- Index . . . . . 281**

# List of Abbreviations

## *Acronyms*

2D BM	2D Bernoulli Distribution Mixture Model
2D CAR	2D Causal Auto-Regressive Model
2D DM	2D Probabilistic Discrete Mixture Model
2D GM	2D Gaussian Mixture Model
2D GMRF	2D Gaussian Markov Random Field
3D CAR	3D Causal Auto-Regressive Model
3D CMRF	3D Compound Markov Model
3D GMRF	3D Gaussian Markov Random Field
3D NCMRF	3D Partially Non-parametric Compound Markov Model
3D PCMRF	3D Potts Compound Markov Model
3D PMRF	3D Gaussian Pseudo-Markov Random Field
3D SAR	3D Simultaneous Auto-Regressive Model
ABRDF	Apparent Bidirectional Reflectance Distribution Function
BDTF	Bidirectional Dynamic Texture Function
BRDF	Bidirectional Reflectance Distribution Function
BRTTF	Bidirectional Reflectance Transmittance Texture Function
BSDF	Bidirectional Scattering Distribution Function
BSSRDF	Bidirectional Surface Scattering Reflectance Distribution Function
BTDF	Bidirectional Transmittance Distribution Function
BTF	Bidirectional Texture Function
CAR	Causal Auto-Regressive
CN	Contextual Neighborhood
CPU	Central Processing Unit
DPI	Dot Per Inch
DMT	Dynamic Multispectral Texture
DT	Dynamic Texture

EM	Expectation Maximization algorithm
FFT	Fast Fourier Transformation
FIR	Finite Impulse Response
GL	Gaussian–Laplacian pyramid
GPU	Graphics Processing Unit
GRF	General Reflectance Function
HDR	High Dynamic Range
IBRDF	Isotropic Bidirectional Reflectance Distribution Function
K-L	Karhunen–Loeve expansion
LDR	Low Dynamic Range
LDS	Linear Dynamical System
LED	Light Emitting Diode
LOD	Level Of Details
LTS	Local Texture Space
MAE	Mean Average Error
MCMC	Markov Chain Monte Carlo methods
MDS	Multi-Dimensional Scaling
MRF	Markov Random Field
MSE	Mean Squared Error
NR	Near-Regular texture
PCA	Principal Component Analysis
PSNR	Peak Signal-to-Noise Ratio
RBF	Radial Basis Functions
RGB	Red, Green, and Blue color space
SLF	Surface Light Field
SNR	Signal-to-Noise Ratio
SRF	Surface Reflectance Field
SSIM	Structure Similarity Index Metric
ST	Static Multispectral Texture
STAR	Spatio-Temporal Autoregressive model
SVBRDF	Spatially Varying Bidirectional Reflectance Distribution Function
VDP	Visual Difference Predictor
VR	Virtual Reality

*Basic Notation and Convention*

$A \setminus B$	set of $A$ elements which are not in $B$
$\mathbf{b}_i, \mathbf{b}_v$	barycentric weights
$\mathbf{B}$	local surface bitangent (orthogonal to normal and tangent)
$D()$	facets distribution function
$E$	expectation
$f_d$	diffuse reflectance
$f_s$	specular reflectance at normal incidence
$F()$	Fresnel function
$G$	graph
$G()$	shadowing/masking function
$H()$	transfer function
$I$	discrete $d$ -dimensional rectangular lattice of $N_1 \times \dots \times N_d$ size ( $N \times M$ for $d = 2$ )
$I_r$	neighborhood system associated with $I$
$I_{(r)}$	discrete rectangular lattice $I$ except the site $r$
$I_r^*$	non-symmetric half-plane of $I_r$
$I_r^u$	unilateral neighborhood
$I_r^c$	causal neighborhood
$I_r^2$	the second-order hierarchical neighborhood
$k_d$	diffuse coefficient
$k_s$	specular coefficient
$L$	radiance/random field, line field
$M$	number of rows
$\mathbf{M}$	matrix of eigen-vectors weighting coefficients
$N$	number of columns
$\mathbf{N}$	local surface normal (equivalent to $\omega_n$ )
$n$	refraction index
$n_i$	number of spatial illumination angles
$n_l$	number of lobes of a reflectance model
$n_p$	rank of polynomial
$n_v$	number of spatial viewing angles
$R_e$	autocovariance function
$S_Y$	spectral density function
$(s, t)$	texture mapping coordinates
$\mathbf{T}$	local surface tangent
$\mathbf{v}$	vertex coordinate
$\hat{\mathbf{U}}$	a subset of applied eigen-vectors
$\tilde{X}$	corrupted observable image
$\check{X}$	a CMRF control random field
$Y$	random field, true unobservable image
$Y^{(0)}$	random field at fine resolution ( $Y^{(1)}$ coarser resolution)
$Y_r$	random variable at the site $r$
$Y_{(r)}$	random field except the random variable $Y_r$
$\tilde{Y}_r$	centered random variable

$Z$	Gibbs normalization constant
$\mathcal{D}$	intrinsic dimensionality (BTF dimensionality)/ non-negative diagonal matrix containing eigen-values
$\mathcal{E}_V$	class of extreme elements of $\mathfrak{N}_V$
$\mathcal{F}$	Fourier (discrete, continuous) or Z transformation
$\mathcal{L}$	(log-)likelihood function
$\mathcal{N}()$	Gaussian distribution
$\mathcal{R}$	space of real numbers
$\mathcal{Z}$	space of integers
$\alpha$	specular parameter
$\gamma$	parameter vector/guess rate (response to zero stimulus)
$\theta$	elevation angle (measured from surface normal)/parameter vector
$\lambda$	eigenvalue/parameter/miss rate (response to large stimulus)
$\rho()$	autocorrelation, sample correlation function
$\rho$	material albedo coefficient
$\varphi$	azimuthal angle
$\sigma$	width of isotropic specular lobe
$\sigma^2$	variance
$\sigma_x, \sigma_y$	width of anisotropic specular lobe
$\psi$	psychometric function
$\omega = \{\omega_1, \dots, \omega_{N \times M}\}$	the interpretation random vector for the lattice $I$ , $\omega_i \in \hat{\Omega}$
$\omega_i$	illumination (incoming) direction
$\omega_v$	viewing (outgoing) direction
$\omega_h$	half-way direction (between illumination and viewing direction)
$\omega_n$	direction of surface normal
$\omega_t$	transmittance direction (measured from inverted surface normal)
$\omega_r$	direction of an ideal mirror reflection
$\Omega$	a set of all possible configurations of $Y$ on $I$
$\hat{\Omega} = \{\hat{\omega}_1, \dots, \hat{\omega}_K\}$	set of all possible interpretation labels
•	all possible values of the corresponding index
$\otimes$	Kronecker product/convolution operator
$\ \cdot\ $	norm of a matrix

# List of Figures

Fig. 1.1	Brodatz “texture” D44 [1] and two of its cutouts . . . . .	2
Fig. 1.2	Visual textures represent an omnipresent natural part of the real world . . . . .	3
Fig. 1.3	Virtual world visual textures (BTF samples courtesy of the Bonn University) . . . . .	4
Fig. 1.4	An example of view and illumination dependency of a rough texture . . . . .	4
Fig. 1.5	Kobylisy subway station in Prague . . . . .	5
Fig. 2.1	General reflectance model . . . . .	10
Fig. 2.2	A taxonomy of selected reflectance models . . . . .	11
Fig. 2.3	BSSRDF reflectance model . . . . .	13
Fig. 2.4	BRTTF reflectance model . . . . .	13
Fig. 2.5	BTF reflectance model . . . . .	14
Fig. 2.6	SLF reflectance model . . . . .	15
Fig. 2.7	SRF reflectance model . . . . .	16
Fig. 2.8	Static-/dynamic texture . . . . .	17
Fig. 2.9	BSDF reflectance model . . . . .	18
Fig. 2.10	BRDF reflectance model . . . . .	19
Fig. 2.11	BTDF reflectance model . . . . .	20
Fig. 2.12	IBRDF reflectance model . . . . .	20
Fig. 3.1	Examples of significant material appearance change for varying illumination/view directions, as captured for knitted wool and lacquered wood (© [2009] IEEE) . . . . .	27
Fig. 3.2	A gonioreflectometer-based BRDF measurement device by White [143] (© [1998] OSA) . . . . .	29
Fig. 3.3	Principle of gonioreflectometer BRDF measurement [70]. Fixed light source (4) illuminates sample (3) positioned on two tilt (D) and pan (C) rotation stage. A bench (2) with photodetector (I) tilts (B) regarding the base, while the entire base turns around (A) with respect to light (© [2008] OSA) . . . . .	29

Fig. 3.4 Gonioreflectometer at National Metrology Institute of Germany [49] with a line-scan camera for measurement of spectral radiance ( $I$ ) and HDR imaging luminance/color measuring device (2) (© [2012] AIP) . . . . . 30

Fig. 3.5 A parabolic-mirror-based BRDF measurement device by Dana et al. [14] (a) (© [2001] IEEE), principle of the BRDF measurement using a parabolic mirror (b), and the multi-view image seen by the camera (c) (© [2001] IEEE) . . . . . 31

Fig. 3.6 BRDF measurement setup based on two mirrors [32] (© [2008] IEEE) . . . . . 32

Fig. 3.7 Portable BRDF measurement setup based on a hemispherical set of LEDs [5] (© [2008] IEEE) . . . . . 34

Fig. 3.8 The principle of the portable BRDF measurement setup based on condenser lens and its prototype ([10] © 2010 Association for Computing Machinery, Inc. Reprinted by permission) . . . . . 35

Fig. 3.9 (a) BTF CURET measurement setup ([17] © 1999 Association for Computing Machinery, Inc. Reprinted by permission). (b) Examples of CURET BTF images of fabric [12] . . . . . 39

Fig. 3.10 BTF measurement setup of Yale University [48] (with courtesy of P. Belhumeur) . . . . . 39

Fig. 3.11 Acquired BTF images of Yale University (material: *moss*) [135] . 40

Fig. 3.12 An example of light or camera trajectory above the sample during measurement [78] (© [2009] IEEE) . . . . . 40

Fig. 3.13 Measurement setup of the Bonn-System consisting out of an HMI lamp, a CCD camera and a robot arm with a sample holder (*left*). Raw image of corduroy BTF measurement [8] (*right*) ([74] © 2005 Association for Computing Machinery, Inc. Reprinted by permission) . . . . . 41

Fig. 3.14 Gonioreflectometer at UTIA, Academy of Sciences of the Czech Republic [133] . . . . . 41

Fig. 3.15 A spherical dome with 151 cameras for BTF measurement ([74] © 2005 Association for Computing Machinery, Inc. Reprinted by permission) . . . . . 43

Fig. 3.16 Examples of cross-polarization: (a) Non-polarized image, (b) polarization planes aligned  $I_1$ , (c) polarization planes perpendicular  $I_2$ , (d) diffuse component  $I_D$ , (e) specular component  $I_S$  . . . . . 50

Fig. 3.17 Sparse BSSRDF acquisition setup: the laser projector illuminates the target object (resting on the turntable). The scene is observed by the HDR video camera from several positions. The two spot lights visible on both sides of the camera in the *right image* are used to illuminate the object during silhouette detection ([36] © 2004 Association for Computing Machinery, Inc. Reprinted by permission) . . . . . 51

Fig. 3.18 Thin sponge sample rendering using (a) BTF measurements only, (b) BTF combined with global dipole diffusion model, and (c) using BTF combined with a model of local scattering measurements by Tong et al. ([34] © 2005 Association for Computing Machinery, Inc. Reprinted by permission) . . . . . 52

Fig. 3.19 A light-stage setup for face appearance acquisition consisting of 150 lights and 16 cameras ([38] © 2006 Association for Computing Machinery, Inc. Reprinted by permission) . . . . . 55

Fig. 4.1 Gaussian (*left*), Laplacian (*middle*), and Gaussian–Laplacian (*right*) pyramids . . . . . 66

Fig. 4.2 Poisson line tessellation (*left*) colored (*middle, right*) to fit target textures . . . . . 68

Fig. 4.3 Voronoi tessellation into six cells (*left*) and filled with natural stone textures (*right*) . . . . . 69

Fig. 4.4 The generic scheme of a 3D multispectral MRF model. . . . . 70

Fig. 4.5 The generic scheme of a 2D multispectral MRF model . . . . . 71

Fig. 4.6 The 2D hierarchical contextual neighborhood  $I_r^1$  of the first order . . . . . 72

Fig. 4.7 The 3D hierarchical contextual neighborhood  $I_r^1$  of the first order . . . . . 73

Fig. 4.8 A wood texture modeled using 2D GMRF and 3D GMRF models 74

Fig. 4.9 Simple 2D causal contextual neighborhood  $I_r^c$  . . . . . 74

Fig. 4.10 Synthetic (3D NCMRF model) enlarged color maple bark texture estimated from its natural measurement (*left column*) . . . . . 79

Fig. 4.11 Synthetic (3D PCMRF model) color lichen texture estimated from its natural measurement (*left column*) . . . . . 80

Fig. 4.12 The Bernoulli mixture model canvas synthesis (*right*) . . . . . 84

Fig. 4.13 The Bernoulli mixture model textile synthesis (*right*) . . . . . 85

Fig. 4.14 The roller enlargement of the rattan texture together with its original measurement (*top*) and the four double-toroid-shaped tiles shown in their original measurement locations. A similar example shows the canvas textures (*bottom*) . . . . . 90

Fig. 4.15 Hybrid texture modeling, target textures (*left*), Gaussian mixture-based gray-scale synthesis (*middle*), and their final hybrid results (*right*) . . . . . 91

Fig. 5.1 Scheme of the proposed dynamic texture hybrid model (© [2006] IEEE) . . . . . 104

Fig. 5.2 The mean (rows 1, 2) and variance (rows 3, 4) images comparison of original (rows 1, 3) and synthesized DT (rows 2, 4) (© [2006] IEEE) . . . . . 105

Fig. 6.1 A BRDF parameterization scheme . . . . . 120

Fig. 6.2 BRDF representation as illumination and view-direction-dependent image (a). Each direction is parameterized by two spherical angles  $\theta/\varphi$ . Angularly uniform sampling (b) and hemispherically uniform sampling (c) . . . . . 122

Fig. 6.3	Half-angle BRDF representation [61] (a) parameterizes BRDF by spherical angles of half-angle direction ( $\theta_h/\varphi_h$ ) with regard to surface normal, and of illumination direction ( $\theta_d/\varphi_d$ ) with regard to the half-angle. Parameterized BRDF (b) allows straightforward isotropy enforcement (c) . . . . .	122
Fig. 6.4	Onion slices BRDF representation [23] divides the hemisphere of illumination directions into a set of parallel ( $\alpha$ ) and meridian ( $\beta$ ) cuts (a). The viewing direction is parameterized by spherical angles $\theta_v/\varphi_v$ . This parameterization divides BRDF into illumination-dependent (b) or view-dependent (c) blocks . . . . .	123
Fig. 6.5	Example of anisotropic BRDF reconstruction from continuous slices: (a) original, (b) sparse-sampling by eight slices, (c) reconstructions of elevations where the slices were measured, (d) missing data interpolation . . . . .	123
Fig. 6.6	Scheme of light interaction at the air-material interface. $\omega_h$ is the halfway vector, $\omega_r$ mirror direction, $\omega_t$ transmission direction	127
Fig. 6.7	A Phong shading example on specular parts of a car gearbox . . .	129
Fig. 6.8	Effects of light interacting with V-shape micro-facet representing material surface . . . . .	132
Fig. 6.9	An example of Kurt's model application for fitting of the pearlescent paint BRDF applied on an upholstery part of armchair 3D model . . . . .	135
Fig. 6.10	Comparison of measured lacquered wood BRDF and its fitting by a model . . . . .	138
Fig. 6.11	SVBRDF estimated for varying illumination as a mixture of known target (a) BRDFs. The principle of the measurement procedure (b), and the complete setup (c) ([58] © 2011 Association for Computing Machinery, Inc. Reprinted by permission) . . . . .	140
Fig. 7.1	Two BTF representations illustrated on [78] measurements (© [2009] IEEE) . . . . .	148
Fig. 7.2	A basic taxonomy of BTF compression and modeling methods . .	149
Fig. 7.3	The 30 highest eigenvalues plotting for eight distinct BTFs . . . .	151
Fig. 7.4	A psychophysical experiment principle. Numbers of preserved images for individual tested materials . . . . .	152
Fig. 7.5	An example of BTF image misalignment due to structural occlusions . . . . .	154
Fig. 7.6	Comparison of reciprocal BRDF vs. non-reciprocal apparent BRDF (ABRDF) data . . . . .	154
Fig. 7.7	BTF compression by means of SVD linear factorization . . . . .	157
Fig. 7.8	BTF compression by means of PCA linear factorization . . . . .	157
Fig. 7.9	A generic BTF model . . . . .	161
Fig. 7.10	A taxonomy of BTF modeling methods . . . . .	162
Fig. 7.11	BTF tiling and quilting principles . . . . .	164

Fig. 7.12 A BTF textile material  $192 \times 192$  (*upper left*), the resulting double toroid-shaped patch template (*bottom left*), four double toroid-shaped patches (*bottom left*), and the enlarged ( $512 \times 512$ ) texture for one illumination- and viewing-angle combination . . . 165

Fig. 7.13 A shell model rendered with the BTF sponge surface material, one Yale University sponge measurement and its detected double toroid-shaped patch (both enlarged and not corresponding to the shell scale) . . . . . 166

Fig. 7.14 Computation of polynomial coefficients . . . . . 167

Fig. 7.15 Comparison of the original BRDF (*solid line*), the BRDF approximated by one-lobe Lafortune model (LM) (*blue, dashed line*) and finally the BRDF approximated by proposed polynomial extension (PLM) (*red, dash-dot line*) for knitted wool material for  $SRF_v - \theta_v = 60^\circ, \phi_v = 54^\circ$  . . . . . 168

Fig. 7.16 Synthesized BTF examples for *knitted wool* and *proposte* materials, respectively. The *first row* describes the mutual positions of light (*empty circle*) and camera (*filled circle*) above the sample; the *second row* shows the original raw BTF data; the *third row* shows the results of one-lobe LM on registered BTF data; and finally, the *fourth row* illustrates the results of the proposed PLM (© [2004] IEEE) . . . . . 169

Fig. 7.17 Image stitching. The source image is cropped from the right along the minimum-error path and placed over the target background image . . . . . 169

Fig. 7.18 The MAE of clustered one-lobe Lafortune model (LM-C—*blue line*) and its clustered polynomial extension (PLM-C—*red line*), compared with the non-clustered variants of LM and PLM (*dash-dot lines*) for all 81 reflectance fields in two BTFs: *knitted wool* and *wood dark* . . . . . 171

Fig. 7.19 Part of a car gearbox covered using four BTFs: *leather dark, wood dark* and *leather dark, wood dark*. The *first row* illustrates the original tiled BTF data, the *second row* depicts the approximation using one-lobe LM, the *third row* is a result of the proposed one-lobe PLM model, the *fourth row* shows the result of the proposed clustered PLM-C model . . . . . 173

Fig. 7.20 Three examples of car interior modeling. These images illustrate seven different materials approximated by means of the proposed reflectance BTF model (PLM-C) . . . . . 174

Fig. 7.21 General schema of a statistical BTF model . . . . . 175

Fig. 7.22 Cushion fabric and foil BTF examples (*odd rows*) for three different illumination angles and their synthetic (*even rows*) results . . . . . 176

Fig. 7.23 An overall schema of the BTF MRF model . . . . . 178

Fig. 7.24 Sub-space index tables for eight materials in two rows: fabrics, leathers, artificial leather, lacquered woods and wool (© [2007] IEEE) . . . . . 179

Fig. 7.25	Normal and range maps (the <i>second</i> and <i>third</i> rows) estimated using photometric stereo and global integration techniques for six materials from the University of Bonn BTF database ( <i>fabric dark, fabric light, leather dark, leather light, leather real and knitted wool</i> ) together with <i>cushion fabric</i> from the UTIA rough texture database . . . . .	180
Fig. 7.26	Results of BTF synthesis mapped on part of a car interior. The original BTF data ( <i>left</i> ), the BTF synthesis ( <i>right</i> ). Tested materials: <i>lacquered woods, tile and plastic flooring</i> (© [2007] IEEE) . . . . .	182
Fig. 7.27	Results of BTF synthesis mapped on part of a car interior. The original BTF data (enlarged by image tiling) (the <i>first</i> column), smooth part of the proposed BTF synthesis (the <i>second</i> row), relighted range-map ( <i>third</i> row), a combination of synthesized data with the range-map ( <i>fourth</i> row). Materials from the <i>left</i> are: two leathers <i>leather dark, leather light</i> , three fabrics <i>fabric dark, fabric light, knitted wool</i> (© [2007] IEEE) . . . . .	183
Fig. 7.28	BTF measurements mapped on part of a car gearbox. Original BTF data (enlarged using image tiling) (the <i>top</i> row) compared with synthesized BTF (the <i>bottom</i> row) for four distinct materials: <i>wood light, leather light, wood dark, leather dark</i> (© [2007] IEEE) . . . . .	184
Fig. 7.29	BTF ceiling panel texture measurements ( <i>upper</i> row) and their synthetic (3D NCMRF) counterparts ( <i>bottom</i> row) for various elevation ( $\theta_i$ ) and azimuthal ( $\phi_i$ ) illumination angles and a fixed viewing angle . . . . .	185
Fig. 7.30	A ceiling panel texture measurement, its synthetic control field, and the final synthetic 3D PCMRF model texture . . . . .	186
Fig. 7.31	Example of stimulus showing original ( <i>left</i> ) and improperly parameterized ( <i>right</i> ) sample <i>synthetic leather</i> (© [2009] IEEE) . . . . .	193
Fig. 7.32	Psychometric functions fitted to the data obtained from the psychophysical experiment for six different BTF samples and three different compression methods: ( <i>top</i> ) per-view BTF images PCA [78], ( <i>middle</i> ) all BTF images PCA [48], ( <i>bottom</i> ) per-pixel BRDF clustering + local PCA [46] (© [2009] IEEE) . . . . .	194
Fig. 7.33	The comparison of individual pixel-wise BTF modeling methods for six different material samples in terms of MAE in CIE Lab color space dependent on viewing direction change (see Fig. 3.12) 0—the top, 81—the bottom of the hemisphere (© [2009] IEEE) . . . . .	196
Fig. 7.34	BTF results of all eight compared methods mapped on a car gearbox console for six different tested materials. Light position: right-back (© [2009] IEEE) . . . . .	198

Fig. 7.35 The comparison of compression ratios dependent on BTF resolution, number of illumination/view directions, and preserved principal components, respectively, for the tested pixel-wise compression methods (©[2009] IEEE) . . . . . 200

Fig. 7.36 Example of standard (BTF compression ratio ~1:10) and clustered (BTF compression ratio ~1:100) PLM RF model compared with probabilistic model 2D CAR (BTF compression ratio ~1:70000) for *lacquered wood* sample (© [2009] IEEE) . . . 201

Fig. 8.1 Example of bidirectional material appearance visualization steps: (a) input data—polygon geometry and texture, (b) texture mapping using fixed local texture space (LTS) per triangle, (c) texture mapping using interpolated LTS across polygons using barycentric coordinates, (d) the same as (c) but with additional interpolation of the measured directions using barycentric coordinates . . . . . 212

Fig. 8.2 Texture mapping principle on geometry represented by triangular polygons . . . . . 213

Fig. 8.3 World vs. local coordinate systems . . . . . 214

Fig. 8.4 Local texture system specified at each vertex of the object’s geometry . . . . . 214

Fig. 8.5 Interpolation of local texture system within the triangle using the barycentric coordinates . . . . . 216

Fig. 8.6 Estimated range map (*left*) and a principle of bump mapping (*right*) . . . . . 218

Fig. 8.7 Subtraction of bump shifted towards light source from original bump produces visual perception of lit bump . . . . . 218

Fig. 8.8 Bump mapping (*left*) vs. Displacement mapping (*right*) for *leather light* material (static texture with only diffuse lighting) . . . 219

Fig. 8.9 Angular interpolation of measured bidirectional reflectance data . . . . . 221

Fig. 8.10 Angular interpolation of measured bidirectional reflectance data beyond measured interpolation . . . . . 221

Fig. 8.11 Indexing of cubemap with precomputed interpolation indices and barycentric weights . . . . . 221

Fig. 8.12 Effect of illuminated area foreshortening captured in BTF of leather material sample. The image shows mean BRDF luminance averaged across all texels . . . . . 223

Fig. 8.13 Illumination environment represented by 128 directional lights (*grace* environment, courtesy of P. Debevec) . . . . . 224

Fig. 8.14 Comparison of point-light and environmental illumination (*grace* environment, courtesy of P. Debevec) . . . . . 225

Fig. 8.15 BTF of corduroy material illuminated by a point light and two different illumination environments (*grace* environment, courtesy of P. Debevec) . . . . . 225

Fig. 8.16 Aliasing on visualization of corduroy material: (a) no anti-aliasing, (b) anti-aliasing using ten mip-map levels . . . . . 226

Fig. 9.1 Problem of texture model validation. When are two textures considered visually similar or identical? This example compares a shape covered by a measured BTF (*top-left*) with the result of a pixel-wise compression (*top-right*), and the result of a probabilistic modeling (*bottom*) . . . . . 232

Fig. 9.2 Example of VDP performance comparing measured and synthesized BTF data . . . . . 234

Fig. 9.3 An example of SSIM comparison for different BTF compression methods performance with original rendering . . . . . 235

Fig. 9.4 Texture comparison by selected image quality metrics on a reference texture (*left*, size  $331 \times 248$  pixels) modified by six different filters. The comparison is relative only; therefore, outputs of individual metrics are normalized to range (0, 1), where 1 corresponds to the highest similarity and 0 to the lowest similarity . . . . . 236

Fig. 9.5 Scheme of psychophysical visual experiment (1) and psychophysically derived model (2) . . . . . 238

Fig. 9.6 Examples of (a) 2-AFC and (b) 4-AFC experimental stimuli . . . . . 240

Fig. 9.7 A typical psychometric function . . . . . 241

Fig. 9.8 Comparison of original BTF illumination/view hemisphere sampling (*left*), with three other sampling approaches ([13] © 2008 Association for Computing Machinery, Inc. Reprinted by permission) . . . . . 246

Fig. 9.9 Psychometric functions showing subjects' visual sensitivity to (*left*) different environment, (*right*) different shapes . . . . . 246

Fig. 9.10 Examples of BTF visual equivalence for two samples, different objects and illuminations ([11] © 2008 Association for Computing Machinery, Inc. Reprinted by permission) . . . . . 247

Fig. 9.11 Resulting sparse sampling (*green dots*) after perceptually thresholded vector quantization of BTF images. Different BTF samples require different sampling (an example of viewing direction distributions with a fixed illumination for corduroy and leatherette *on the right*) . . . . . 248

Fig. 9.12 Results of the eye-tracking across different materials: (a) average subjects response success rate, (b) average stimulus duration [ms], (c) average number of fixations, and (d) average fixation duration [ms] (With kind permission from Springer Science and Business Media [16], 2012) . . . . . 249

Fig. 9.13 Results of the psychophysical study with interactive BTF stimuli . . . . . 250

Fig. 10.1 Overview of texture applications . . . . . 256

Fig. 10.2 Wood and tile natural textures and their resynthesized edited counterparts using the 3D CAR models (*right*) ([30] © 2009, with kind permission from Springer Science and Business Media) . . . . . 257

Fig. 10.3 Edited near-regular texture BTF fabric in the background and golden lattice in the foreground (*left*) and BTF sponge and green plastic combined materials (*right*) . . . . . 258

Fig. 10.4 Measured and synthetic edited color maple bark (*upper right*) with some texture sub-models learned on the *yellow* flowering shrub texture (*bottom*) ([33] © 2012, with kind permission from Springer Science and Business Media) . . . . . 258

Fig. 10.5 Controllable Markovian edge detector applied to a zebra image . . 260

Fig. 10.6 Large (8000 × 8000 pixels) aerial image (*left*) unsupervised segmentation (*right*) . . . . . 260

Fig. 10.7 Range scene (*left*) with general face objects segmentation (*right*) (© range and intensity image USF, <http://marathon.csee.usf.edu/range/DataBase.html>) . . . . . 261

Fig. 10.8 Comparison of illumination-invariant texture retrieval between Markovian invariants (*left*) and LBP features (*right*) . . . . . 262

Fig. 10.9 A tile retrieval mobile phone application . . . . . 263

Fig. 10.10 Prague texture segmentation data-generator and benchmark home page and some evaluation details (*right*) . . . . . 264

Fig. 10.11 ALI satellite hyperspectral ( $d = 10$ ) textural mosaic (*left* in pseudocolors), ground truth (*middle*) and the unsupervised classification thematic map (*right*) . . . . . 264

Fig. 10.12 Detected cancer on the craniocaudal patient mammogram . . . . 265

Fig. 10.13 Enhanced malignant mammogram using the log-likelihood model image . . . . . 266

Fig. 10.14 Treatment monitoring (*right*) of the pemphigus vulgaris dermatological disease ([25] © 2007, with kind permission from Springer Science and Business Media) . . . . . 266

Fig. 10.15 Eye and its transformed iris texture . . . . . 267

Fig. 10.16 Car seat triangular model and the paper scrap seat cover . . . . 269

Fig. 10.17 Car industry example . . . . . 270

Fig. 10.18 Celtic druid head (300 BC, National Museum in Prague) from *upper left* to *bottom right* the original head, ABS plastic model based on shape laser measurements, precise BTF planer model, and planer model appearance in an environmental lighting, respectively (*grace* environment, courtesy of P. Debevec) . . . . . 271

Fig. 10.19 Celtic druid head simulated earthenware, and wood material appearance, respectively . . . . . 272

Fig. 10.20 The National Gallery in Prague—Department of Modern Art virtual model . . . . . 272

# List of Tables

Table 3.1	Comparison of public research texture databases . . . . .	25
Table 3.2	Comparison of publicly available BTF databases . . . . .	45
Table 3.3	Comparison of selected SVBRDF and BTF measurement systems parameters . . . . .	46
Table 7.1	The mean average error (MAE) of the synthesized BTFs for one-lobe Lafortune model (LM), its polynomial extension (PLM), and its clustered polynomial extension (PLM-C) . . . . .	172
Table 7.2	The storage size of the proposed PLM and PLM-C in comparison with the size of the raw BTF data and their tiled representation . . . . .	172
Table 7.3	Estimated numbers of PCA components for six different BTF samples with their average and three different tested compression methods . . . . .	195
Table 7.4	Observer’s responses to PTM RF and PLM RF methods and guess rates $\gamma$ for all tested BTF samples . . . . .	195
Table 7.5	Mean Average BTF reconstruction error (in a CIE Lab color-space) of the tested pixel-wise methods . . . . .	197
Table 7.6	Formulas giving the size of parametric representations of the tested pixel-wise methods . . . . .	198
Table 7.7	Size of the parametric representation and compression ratio of the tested methods compared with raw and tiled original BTF data . . . . .	199
Table 7.8	Time demands and computational complexity of analysis and synthesis stages of the tested methods . . . . .	202
Table 7.9	Rough comparison of attributes for the implemented BTF models . . . . .	204

# Chapter 1

## Motivation

**Abstract** Visual information is the most important information on which the majority of all living organisms base their cognition and survival strategy. A visual scene has two important cognitive categories, which are crucial for image understanding: shapes and materials. This book focuses on the latter category—visual aspects of surface materials which manifest themselves as visual textures. Visual texture is of key importance for recognition of objects as well as for estimation of their properties. Pixels, as the basic elements of any digitized visual texture, are known to be highly spatially, and spectrally correlated, but they are also correlated in the time or viewing and illumination angular spaces. Representations of visual textures which respect these multi-dimensional visual space correlations thus form an advantageous foundation for any advanced visual information processing applied to both cognitive (analysis) and modeling (synthesis) purposes.

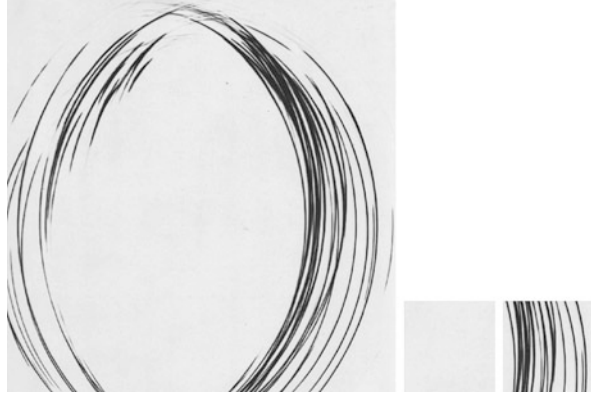
### 1.1 Visual Texture Definition

The notion of texture comes from Latin word *texere* which means to weave; and *textura* is a weaving, web, structure. Its meaning may, according to *Oxford* or *Webster's dictionaries*, be any of these:

- The process or art of weaving; the fabricating or composing of schemes, writings, etc. A woven fabric, or any natural structure having an appearance or consistence as if woven.
- The character of a textile fabric (fine, coarse, close, loose, etc.) resulting from a way in which it is woven.
- The constitution, structure, or substance of anything with regard to its constituents or formative elements.
- Something composed of closely interwoven or intertwined threads, strands, or the like elements.
- The essential part of something, an identifying quality.
- The size and organization of small constituent part of a body or substance; the visual or tactile surface characteristics and appearance of something.

The exact meaning of texture depends on the application area. While in geology it is a physical appearance or rock character, in material science it is a distribution

**Fig. 1.1** Brodatz “texture” D44 [1] and two of its cutouts



of crystallographic orientations, in soil research it describes the proportion of grain sizes, in cosmology it is a type of a topological defect, for artists it is the look and feel of the canvas, for graphic designers it is often any image mapped onto a surface, etc.

Although the notion of visual texture is tied to the human semantic meaning and texture analysis is an important area of image processing, there is no mathematically rigorous definition of texture that would be accepted throughout the computer vision community. Sometimes even its interpretation is subjective. E.g., is the Brodatz [1] texture D44 (Fig. 1.1) really a texture? This image obviously violates the homogeneity condition (see below), if not others as well. Rather than enlarging the list of rather philosophical definitions of texture, we understand a textured image or the *visual texture* to be a realization of a random field, and our effort is simply to find its parameterizations in such a way that the real texture representing certain material appearance measurements will be visually indiscernible from the corresponding random field’s realization, whatever the observation conditions might be. Some work distinguishes between texture and color. We regard such separation between spatial structure and spectral information to be artificial and principally wrong because there is no bijective mapping between grayscale and multi-spectral textures. Thus our random field model is always multispectral.

The notion of a visual texture is based on several ingredients:

*Homogeneity:* A texture is homogeneous if its spatial covariance function is translation invariant.

*Uniform structure:* Texture consists of some uniformly arranged elements (texels or textons). This arrangement is approximately the same everywhere within the textured region.

*Variable reflectance:* Texture is manifested by locally variable reflectance even if it is globally uniformly illuminated.

*Scale dependency:* Based on the resolution scale any surface material can appear as smooth (low resolution) or textured (high resolution).

*Regionality:* Texture is a property of an image region.

*Materiality:* Texture represents a surface material appearance.

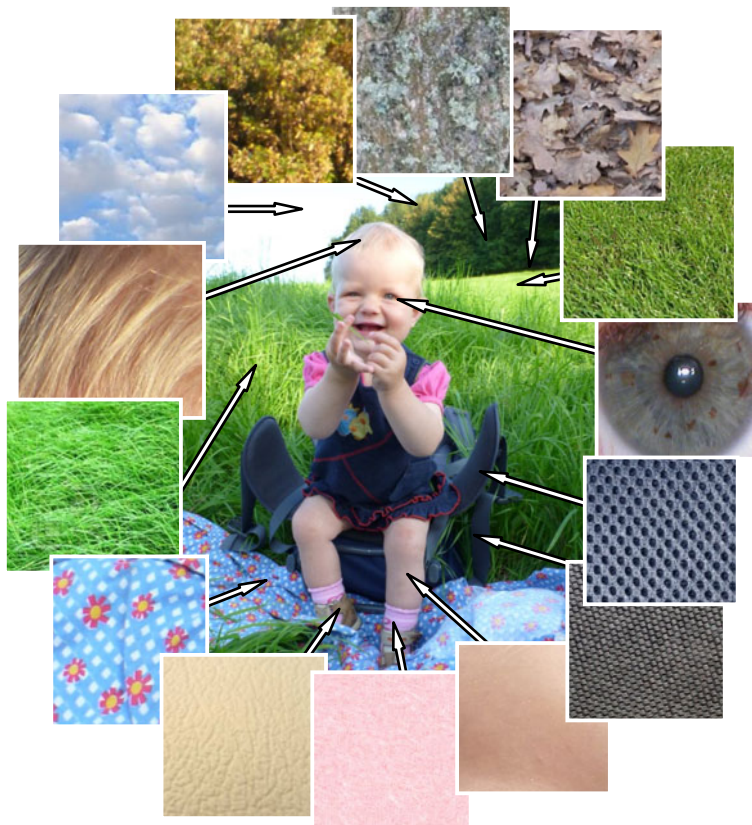


**Fig. 1.2** Visual textures represent an omnipresent natural part of the real world

Visual textures form a natural part of our environment as we are learning to understand, estimate and predict their properties solely based on their visual appearance (Fig. 1.2); however, they are also an integral part of any plausible virtual world (Fig. 1.3).

As appearance of the visual textures depends heavily on the lighting and viewing conditions (Fig. 1.4), this dependency should be taken into account in various application scenarios.

This large range of the real-scene variable illumination and viewing condition is illustrated in the fish-eye image from the Prague Metro (Fig. 1.5). The subway station contains several materials (stone tiles, ceramic tiles, aluminum panels, stainless steel, lacquered iron, glass) and identical illumination lights placed at regular distances. Reflectance variations are clearly visible on floor stone tiles and stainless steel columns as well as on the aluminum wall panels. Even the textile overcoat and leather handbag of the lady standing in the foreground show clear material illumination dependency.